Rare Metal Materials and Engineering
Volume 55, Issue 6, June 2026
Available online at www.rmme.ac.cn

Science Press

Cite this article as: Zhang Liwen, Bian Tianjun, Gong Xiaotao, et al. Effect of Laser Shock Peening on Creep Aging Behavior and Springback of 2195 Al-Li Alloy[J]. Rare Metal Materials and Engineering, 2026, 55(06): 1429-1436. DOI: https://doi.org/10.12442/j.issn.1002-185X.20250294.

ARTICLE

Effect of Laser Shock Peening on Creep Aging Behavior and Springback of 2195 Al-Li Alloy

Zhang Liwen[1], Bian Tianjun[1], Gong Xiaotao[1], Cui Yingguo[1], Song Jiping[2]

[1] Xi'an Aeronautical Polytechnic Institute, Xi'an 710089, China; [2] Chinese Flight Test Establishment, Xi'an 710089, China

Abstract: The impact of laser shock peening (LSP) treatment on the creep aging behavior of 2195 Al-Li alloy was investigated by hardness testing, microstructural characterization, and creep aging forming experiments. Its effect on the springback of single-curved components formed through creep aging was also evaluated. The results indicate that, compared with that of the creep-aged alloy without LSP treatment, the hardness of the creep-aged alloy with LSP treatment is increased by approximately 22%. Grain size is notably reduced from the surface to the middle layer of the plate, with the greatest decrement in surface layer (49 μm) and the least in the middle layer (4 μm). The T1 precipitate phase in the creep-aged alloy with LSP treatment exhibits a denser distribution, greater quantity, and finer grain size, compared with that without LSP treatment. Furthermore, the springback ratio of creep-aged sheets subjected to LSP treatment is significantly lower than that of untreated sheets, decreased by about 37.6%. The enhancement in hardness is attributed to fine grain strengthening and substantial precipitation strengthening induced by LSP. The reduction in springback is ascribed to the increased creep deformation resulting from the combined effect of the compressive stress on the concave surface of the plate during bending and the residual compressive stress generated by LSP treatment.

Key words: LSP; creep aging; springback; precipitation strengthening

1 Introduction

Laser shock peening (LSP) is a surface enhancement technique that uses high-energy pulsed laser beams to generate intense compressive stress waves, inducing plastic deformation on metal surfaces[1]. The working principle involves irradiating an absorption layer (e.g., aluminum foil or black paint) on the metal surface with a high-power-density (GW/cm^2) short-pulse laser (10–30 ns). The absorption layer vaporizes instantaneously under laser irradiation, producing a high-temperature plasma shockwave that acts on the metal surface. As a remote non-contact surface modification technique, LSP avoids thermal damage while refining surface grains, thereby enhancing material strength through grain refinement. Compared to traditional mechanical surface enhancement methods, LSP offers advantages, such as higher peak pressure, non-contact operation, and higher strain rates[2].

Creep aging forming (CAF) is an advanced integrated forming-strengthening technique for aluminum alloy panels, combining creep deformation and aging hardening to simultaneously shape and enhance component performance[3]. With the benefits including integrated forming, performance optimization, short processing cycles, and high dimensional stability, CAF has been already applied in manufacturing aircraft wings and rocket fuel tanks[4–5]. To improve the effectiveness of CAF, extensive researches have focused on pre-treatments applied before CAF process. These primarily include pre-deformation, pre-rolling (at room and cryogenic temperatures), and cyclic loading. For example, Yang et al[6] investigated the effects of pre-deformation on springback, microstructure, and mechanical properties of 2219 aluminum alloy sheets during CAF. They demonstrated that introducing 7% pre-deformation significantly reduces springback, resulting in a post-formed curvature radius closer to the target radius. The overall mechanical properties of the pre-deformed sheets are superior to those of the non-pre-deformed sheets,

Received date: June 27, 2025
Foundation item: University-Level Key Research Projects of Xi'an Aeronautical Polytechnic Institute (24XHZD-02); Youth Innovation Team of Shaanxi University-Aviation Key Structural Parts Precise Control Technology Application Innovation Team (2023-98)
Corresponding author: Zhang Liwen, Ph. D., Associate Professor, Xi'an Aeronautical Polytechnic Institute, Xi'an 710089, P. R. China, E-mail: npuzlw@mail.nwpu.edu.cn

Copyright © 2026, Northwest Institute for Nonferrous Metal Research. Published by Science Press. All rights reserved.

with more uniform property distribution. Compared with non-pre-stretched sheets, the pre-stretched sheets exhibit a 7.3% increase in tensile strength and a 20.8% increase in yield strength, along with a significant reduction in in-plane anisotropy. Xu et al[7] investigated the influence of creep aging temperatures (160–200 °C) and 8% pre-rolling at room temperature on the mechanical properties and microstructure of AA2050 aluminum alloy. They found that for the alloy subjected to 8% pre-rolling, its strength increases initially and then decreases with rising temperature during creep aging. At 180 °C, the synergistic effects of diffusion kinetics and thermodynamic driving forces promote the dense precipitation of T1 phases, resulting in excellent strength. However, when the temperature reaches 200 °C, the activated ledge mechanism leads to significant coarsening of the T1 phases, thereby reducing the strength. Zhu et al[8] investigated the effects of different cryo-rolling pre-deformation levels (20% – 80%) on the stress relaxation aging behavior and mechanical properties of the alloy. The study revealed that compared to T4 treatment, cryo-rolling pre-deformation increases the steady-rate relaxation rate by 35%–360% and effectively prolongs the duration of the variable-rate relaxation stage. Increasing the pre-deformation level significantly enhances the strength of the stress relaxation aged alloy but reduces its elongation. Cryogenic pre-deformation not only promotes the homogeneous precipitation of fine η_2-type phases in the matrix, but also induces the heterogeneous nucleation of relatively large η_2-type phases at dislocations. Zuiko et al[9] investigated the aging response of 2519 aluminum alloy following cyclic strengthening. Their findings revealed that cyclic hardening significantly alters the aging behavior of alloy. The synergistic application of cyclic pre-straining combined with monotonic pre-deformation simultaneously enhances strength and ductility. These improvements in mechanical properties are attributed to microstructural refinement. The repetitive elastic strain applied prior to artificial aging introduces vacancies and dislocations, thereby promoting structural homogenization and substantially increasing the number density and volume fraction of key strengthening phases (θ' and Ω) as well as clusters. Similar results have been found in Al-Zn-Mg-Cu alloy and 2195 Al-Li alloy[10–11]. The aforementioned research confirms that pre-treatments before creep aging substantially affect the creep aging behavior of aluminum alloys. It is particularly noteworthy that recent research indicates that residual compressive stress introduced by machining can reduce the springback of creep-aged sheets[12]. In terms of LSP, it can refine surface grains and achieve fine grain strengthening[13–14], whereas existing methods, such as pre-deformation, rolling, and cyclic loading, fail to achieve this. Additionally, it can also induce residual compressive stress on sheet surfaces[15]. Based on a comprehensive analysis of these findings, LSP pre-treatment is expected to enhance the strength of creep-aged alloys and reduce springback. Based on the above insights, this study proposed an LSP pre-treatment method to reduce springback and enhance the strength of 2195 Al-Li alloy components during CAF, offering a novel approach for precision manufacturing of high-performance and light-weight aerospace panels.

2 Experiment

The commercial hot-rolled 2195 Al-Li alloy sheet with a thickness of 3 mm was selected for this experiment, and its chemical composition is listed in Table 1. Specimens with dimensions of 80 mm×10 mm were prepared for creep aging tests, with their longitudinal direction aligned parallel to the rolling direction. The specimens first underwent solid solution treatment, which were held at 505 °C for 40 min, followed by rapid quenching in room-temperature water. The purpose of solid solution treatment was to dissolve alloying elements into the matrix, forming a homogeneous solid solution and preparing for subsequent aging. Studies indicate that the alloy exhibits the Portevin-Le Chatelier effect in the solid-solution-treated state, significantly impacting structural integrity and surface quality[16–17]. Therefore, after solid solution treatment, the specimens were naturally aged at room temperature for 24 h to stabilize the alloy[18]. The specimens were then divided into two groups: one subjected to LSP treatment and the other remained untreated as a control group. Both groups underwent creep aging tests and microstructural characterization. The overall flowchart of experiment is illustrated in Fig.1.

LSP was performed before CAF tests on the single surface of specimen using a YAG laser apparatus (TYRID Inc, China). Based on the sheet thickness, a relatively low laser pulse energy of 3 J was selected to avoid excessive thermal deformation caused by high energy input. The processing parameters of LSP were set as follows: spot diameter of 3 mm, spot overlap rate of 50%, and pulse width of 10 ns, with water serving as the confinement layer and black tape as the absorbent layer. To ensure treatment effectiveness, each side of the sheet underwent three repeated LSP processes. Prior to the experiment, specimens were polished and ultrasonically cleaned in an ethanol bath. The schematic diagram of sheet with LSP treatment is shown in Fig.2.

Vickers hardness reflects the relationship between the microstructure and mechanical properties of specimens. For

Table 1 Chemical composition of 2195 Al-Li alloy (wt%)

Cu	Li	Mg	Ag	Si	Ti	Fe	Zr	Al
3.87	1.18	0.49	0.41	0.42	0.04	0.04	0.12	Bal.

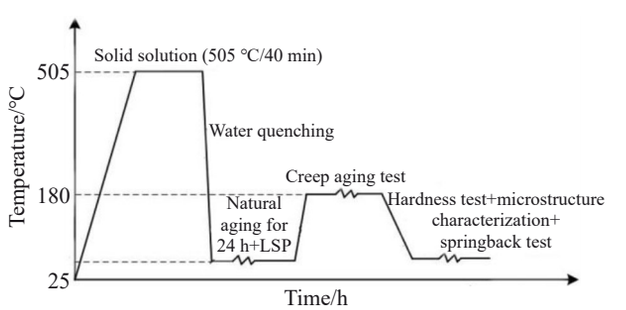

Fig.1 Flow chart of the whole experiment

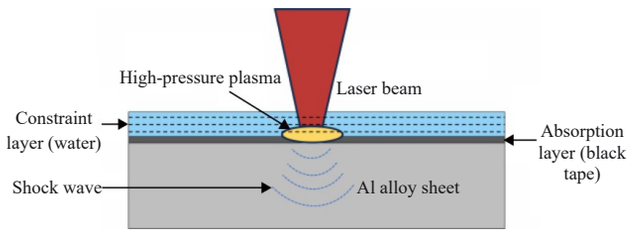

Fig.2 Schematic diagram of sheet with LSP treatment

both LSP-treated and untreated aged alloys, hardness tests were conducted at three positions (1#, 2#, and 3#), as shown in Fig. 3. Following the requirements of GB/T 4340.1-2009, the HVS-1000A Vickers hardness tester was used under the following conditions: load of 1.96 N, dwell time of 10 s, and test spacing of 2 mm. For LSP-treated specimens, measurements were conducted on the laser-shocked surface (the side in contact with the punch die), while untreated specimens were tested on the same mold-contact side. Five measurements were conducted at each location, and the average was calculated to obtain the final hardness value.

To evaluate the effects of LSP on the microstructural morphology and grain size of creep-aged sheets, optical microscope (OM, Olympus BX53) was employed to characterize specimens processed under both conditions. Specimens for characterization were extracted from position 1# (as shown in Fig. 3), with dimensions of approximately 5 mm×5 mm×1.5 mm (half of the sheet thickness). These thin sections were sequentially ground using 500#, 1000#, and 3000# water-abrasive sandpapers, followed by mechanical polishing with silica suspension to achieve a mirror-like finish. Finally, the specimens were etched with Keller ' s reagent (2.5vol% HNO_3+1.0vol% HF+1.5vol% HCl+95vol% H_2O) for 10 s[19–20]. To investigate the nano-scale precipitation behavior of the heat-treated Al-Li alloy under both processing conditions, scanning transmission electron microscope (STEM) was used to observe the nano-sized precipitates. Specimens for STEM analysis were obtained from position 1# in Fig. 3, with dimensions of 5 mm×5 mm×0.5 mm. STEM specimen preparation involved grinding the speciment until its thickness was 50 μm using 2000# water-abrasive paper and electrolytic double-jet thinning at − 10 °C and 20 V in an electrolyte to prepare a thin film with a diameter of approximately 3 mm[21–22].

The creep aging experiment involved three steps. (1) Loading and fitting to tool surface: both LSP-treated and untreated sheets were placed on a lower tool. A punch die was pressed downward to tightly fit the sheet against the lower die. (2) Creep aging: after loading, the mold assembly (Fig.4) was secured with bolts and nuts, and then heated to the optimal aging temperature of 180 °C for the Al-Li alloy in a furnace at a rate of 2 °C/min. The temperature was maintained for 12 h. (3) Unloading and springback measurement: after cooling, the bolts were loosened to allow the creep-aged sheet to springback freely. Springback amount ($\Delta H=H-H'$) and springback ratio ($\delta=\Delta H/H$) were measured according to Fig.5, where H represents the initial maximum chord height (approximately 18 mm) after tool loading, and H' denotes the post-unloading chord height.

Notably, LSP-treated surface was aligned with the convex mold during loading to minimize springback. This strategy leveraged the residual compressive stress induced by LSP, which combined with the compressive stress on the concave side during bending. The superimposed stresses enhanced creep deformation and reduced springback.

3 Results and Discussion

3.1 Hardness

The hardness of metallic materials indirectly reflects their strength, with higher hardness values generally indicating superior material strength. Fig. 6 illustrates the hardness variations of creep-aged specimens (at positions shown in Fig. 3) with and without LSP treatment. Notably, the hardness of the LSP-treated alloy is significantly higher than that of the untreated alloy. Additionally, minimal variation in hardness was observed among positions 1#, 2#, and 3# after both processing routes. Specifically, the average hardness of the LSP-treated alloy is approximately 158 HV, compared to that of the untreated alloy (129 HV), representing a hardness improvement of approximately 22%. These results

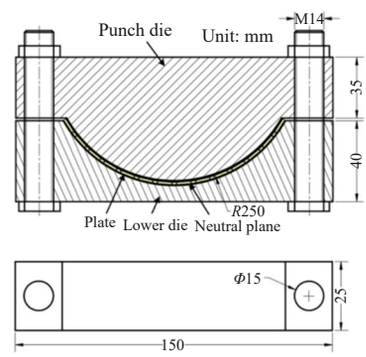

Fig.4 Assembly diagrams of CAF

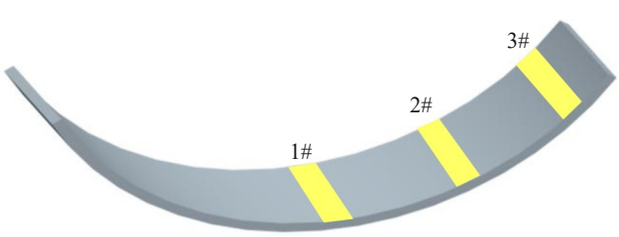

Fig.3 Schematic diagram of sampling location for hardness test

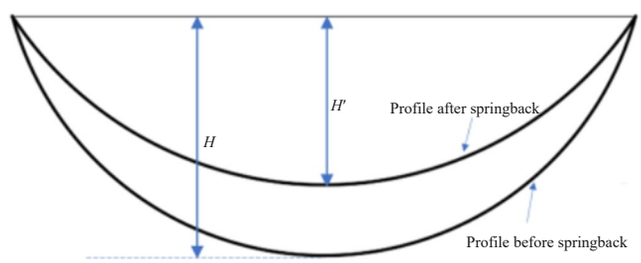

Fig.5 Schematic diagram of plate springback

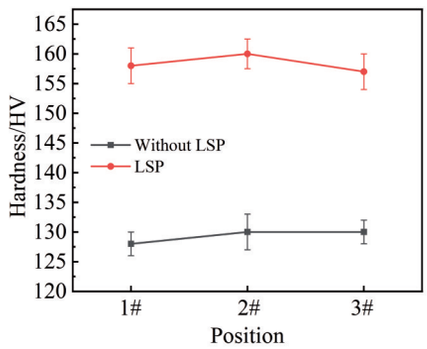

Fig.6 Hardness values of creep-aged alloys with and without LSP treatment

demonstrate that LSP pre-treatment of the initial sheet surface prior to creep aging enhances the hardness and strength of the alloy. The observed experimental outcomes are closely linked to the microstructural evolution of the alloy under the two processing routes. Therefore, a detailed microstructure analysis of the post-processed sheet is necessary.

3.2 Microstructure

Fig. 7 presents the original grain morphology before LSP treatment, revealing that the grain size gradually increases from the surface layer to the intermediate layer, forming a gradient distribution. This microstructure results from the hot-rolling process of the original plate. Furthermore, comparison of grains between LSP-treated alloys (Fig. 8a) and the untreated alloys (Fig.7) reveals no significant changes in grain morphology or size. This confirms that creep aging alone has minimal effect on grain structure. Fig.8 shows OM images of creep-aged alloys without and with LSP treatment. Under both conditions, grain size also exhibits gradient distribution from the surface layer to the intermediate layer, with finer grains in the surface and coarser grains in the intermediate layers. For the untreated alloy (Fig. 8a), the surface layer undergoes recrystallization due to severe plastic deformation induced by hot rolling, while the intermediate layer retains larger grains owing to restricted plastic deformation and low stored energy. In contrast, LSP-treated alloy (Fig. 8b) displays significantly reduced grain sizes, particularly at the surface.

To quantify these differences, the cross-section is divided into six equidistant regions (indicated by the division areas 1–6 in Fig.8) from the surface to the intermediate layer. Image-Pro Plus analysis software was used to calculate average grain sizes (Fig. 9). The specimens underwent standard metallographic preparation (sectioning, mounting, grinding, and polishing) and were then etched with Keller's reagent to clearly reveal the grain boundaries. Representative OM images from different fields of view were subsequently acquired using OM at 200× magnification. To ensure statistical representativeness, at least three images per specimen, covering different regions, were captured. The acquired raw OM images were first processed using the Image-Pro Plus software to enhance the contrast between the grain boundaries and the grain interiors. Using the particle analysis function within the software, individual grain regions were automatically identified and labeled based on the processed binary images (where grain boundaries act as separators). This analysis was then used to calculate geometric characteristic parameters (equivalent circle diameter, namely

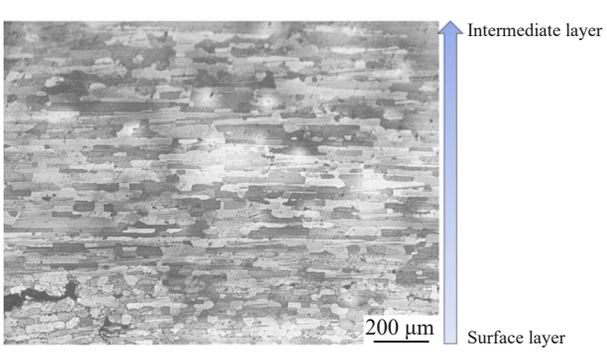

Fig.7 Original grain morphology of 2195 Al-Li alloy before LSP treatment

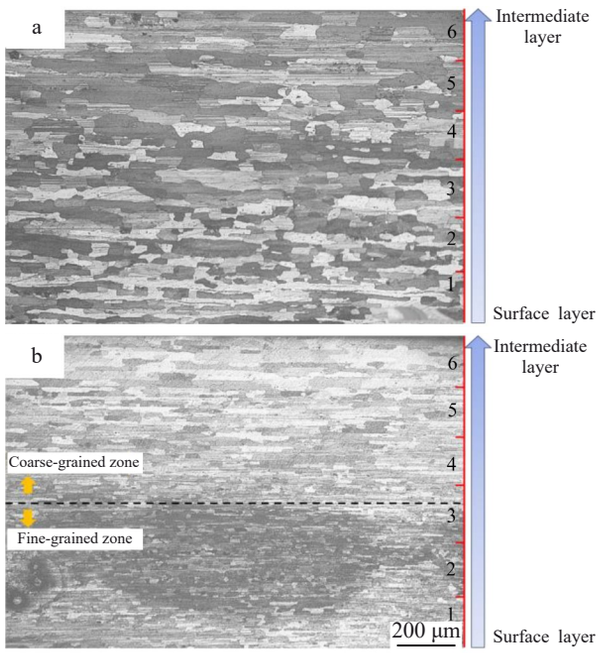

Fig.8 OM images of creep-aged alloys without (a) and with (b) LSP treatment

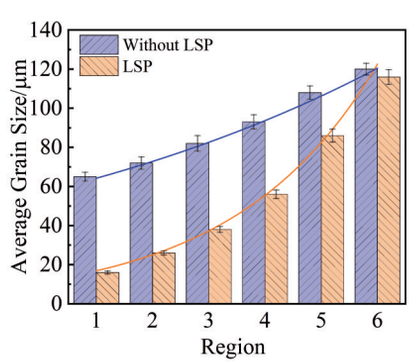

Fig.9 Average grain size in different regions of creep-aged alloys with and without LSP treatment

average grain size) for each identified grain. It can be seen from Fig. 9 that the LSP-treated alloy exhibits smaller grains across all regions compared to the untreated alloy. The maximum grain size difference ($\Delta D=D_0-D_L$, where D_0 and D_L represent the grain size of untreated and LSP-treated specimens, respectively) is 49 μm at the surface (Region 1), decreasing to 4 μm at the intermediate layer (Region 6). This gradient reduction in grain size disparity is attributed to two factors: LSP-induced fragmentation of coarse grains and dynamic recrystallization during creep aging (180 °C) in surface regions subjected to severe plastic deformation and high strain energy. The intermediate layer, less affected by LSP, has relatively stable grain sizes. According to the Hall-Petch relationship[23–24], fine grains enhance material strength and hardness. Thus, the superior hardness of the LSP-treated alloy (Section 3.1) partially originates from grain refinement, especially in surface regions. Additionally, differences in nano-scale precipitation behavior during creep aging may further influence hardness, necessitating detailed precipitate characterization (Section 3.3).

3.3 Precipitation behavior

The influence of LSP treatment is the most pronounced on the metal surface layer, which can be confirmed by Fig. 8. Its effects extend to a depth of approximately 600 μm below the surface. To ensure clear microstructural contrast and highlight the impact of the LSP process on the precipitation behavior of alloy, all STEM specimens were prepared by sectioning material at a thickness of 200 μm below the surface at identical locations (position 1#), as shown in Fig. 3. Fig. 10 presents the selected area electron diffraction (SAED) patterns and morphologies of nano-sized precipitates in creep-aged alloys with and without LSP treatment. SAED patterns (Fig. 10a – 10b) reveal that the primary precipitates in both processing routes are T1 (Al_2CuLi) phases, which significantly contribute to strengthening[25–26]. High-angle annular dark-field (HAADF) images (Fig. 10c – 10d) further demonstrate that the nano-precipitates in both alloys consist of T1 phases with two distinct variants. Compared to the untreated alloy, the creep-aged alloy with LSP treatment exhibits a higher density and finer distribution of precipitates.

Quantitative statistical analysis of precipitate size using Image-Pro Plus software (Fig. 11) shows that the average size of T1 phases decreases from 126 nm in the untreated alloy to 51 nm in the LSP-treated alloy, representing a 59.5% reduction. Studies indicate that finer and denser precipitates can hinder dislocation motion more effectively[27–28]. When dislocations encounter precipitates, they must overcome additional resistance proportional to the size and density of the precipitates. Smaller and more numerous precipitates impede dislocation bypassing or shearing, thereby enhancing material strength and indirectly increasing hardness. These findings align with the 22% hardness improvement observed in Section 3.1 for the LSP-treated alloy.

Under the assumption of pure bending, the stress (σ) at a given position in the sheet (for the same process, i.e., with or without LSP treatment) remains theoretically consistent, as derived from the Eq. (1):

$$\sigma=Ey/\rho \quad (1)$$

where E is the elastic modulus, ρ is the die radius, and y is the distance from the intermediate layer. Thus, it is reasonable to deduce that the hardness of the alloy after creep aging under identical stress and temperature conditions should exhibit minimal variation. This deduction aligns with the consistent hardness values observed across different positions in Fig.6.

3.4 Strengthening mechanism

As shown in Fig. 12, the enhancement of alloy strength is attributed to the synergistic effects of grain refinement strengthening and precipitation strengthening. The resistance of metallic materials to plastic deformation is fundamentally influenced by their microstructural characteristics. Grain boundaries serve as effective barriers to dislocation motion, necessitating increased applied stress for deformation initiation, with refined grain structures significantly enhancing

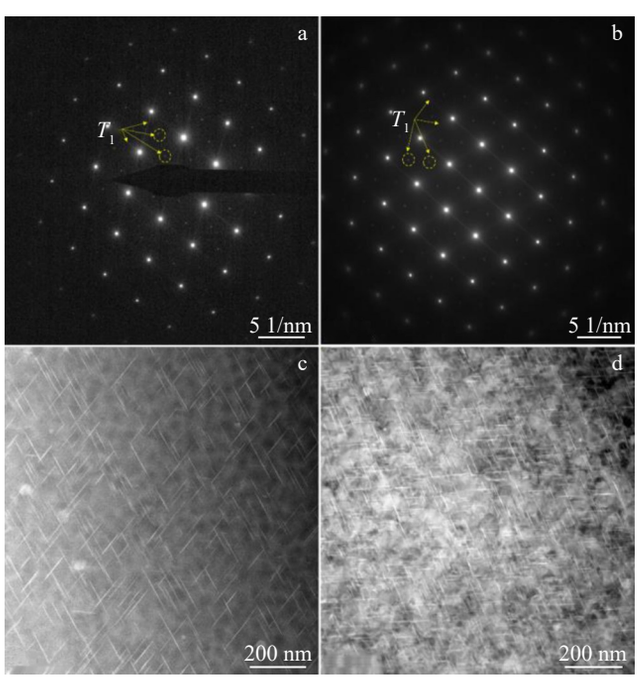

Fig.10 SAED patterns (a–b) and HAADF images (c–d) of creep-aged alloys without (a, c) and with (b, d) LSP treatment

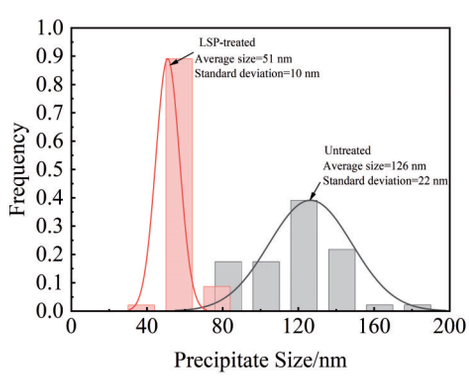

Fig.11 Precipitate size distribution of creep-aged alloys with and without LSP treatment

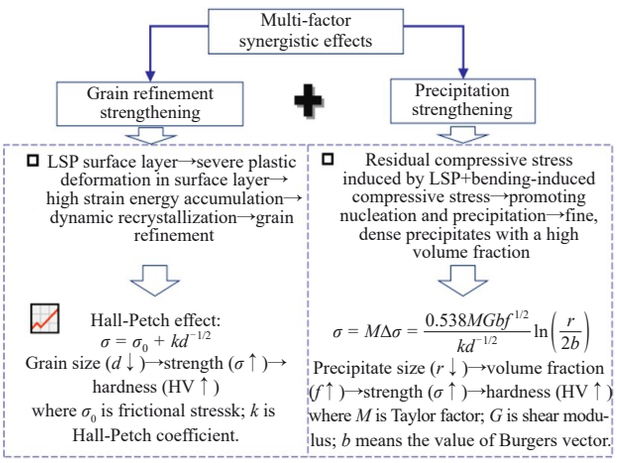

Fig.12 Schematic diagram of strengthening mechanisms in creep-aged Al-Li alloy

hardness and indentation resistance through the Hall-Petch mechanism. Regarding the detailed mechanisms of LSP-induced grain refinement, the powerful shock wave pressure generated by laser impact instantaneously exceeds the dynamic yield strength of material, inducing intense and inhomogeneous plastic flow within the surface layer (typically to depths of several hundred micrometers). Under ultrahigh stress, massive dislocations are activated, multiplied, and glided along slip systems. The extremely high strain rate and complex stress state (high pressure+shear) hinder dislocation motion, rapidly leading to dislocation interactions, tangling, and pile-ups, and forming high-density dislocation walls[29–30]. These dislocation walls subdivide the original grains into finer regions with slightly different orientations, namely dislocation cells or subgrains. Furthermore, ultrahigh-strain-rate plastic deformation generates immense distortion energy and an extremely high dislocation density (reaching 10^{16}–10^{17} m^{-2})[30]. Concurrently, part of the plastic deformation work is converted into thermal energy (adiabatic heating), causing an instantaneous temperature rise in the deformation zone (up to 30%–50% of the melting point of material, yet still well below it) [31]. Combined with the subsequent moderate-temperature (180 °C) environment provided by creep aging, these conditions of high distortion energy and moderate temperature facilitate dynamic recovery and enable grain refinement to be ultimately achieved.

It is worth mentioning that the process combines LSP at room temperature with subsequent creep aging at 180 °C. LSP induces significant grain refinement in the surface layer. During the subsequent aging at 180 °C, further grain refinement is generally not achieved and may even induce partial recovery or substructure coarsening. However, the initial fine-grained structure formed by LSP in the surface layer, particularly within the near-surface region, is largely preserved. The final grain size remains significantly smaller than that of the original material. The primary purpose of aging at 180 °C is precipitation strengthening and creep deformation, rather than further refinement. For age-hardening alloys, the pinning effect of precipitate is key to stabilize the refined microstructure. Although minor recovery and local coarsening can occur, the overall microstructure (grain/subgrain) is still substantially refined. Through the above process, a layer of fine-grained (<20 μm) microstructure is formed on the material surface. Compared with creep-aged alloy without LSP treatment, the surface grains of LSP-treated alloy show a maximum reduction of 75.4% in size. This fine-grained structure introduces a high density of high-angle grain boundaries, which effectively impedes dislocation motion and significantly strengthens the material via the Hall-Petch effect. Concurrently, the precipitation strengthening effect manifests through two distinct mechanisms when precipitate sizes are reduced (e.g., T1 phase refinement from 126 nm to 51 nm in this study). For incoherent precipitates, dislocations circumvent these obstacles via the Orowan bypass mechanism, bowing around particles and requiring elevated stress levels. Conversely, coherent T1 precipitates permit dislocation shearing through the particles themselves, with the cutting process generating additional resistance through interfacial energy dissipation and lattice distortion effects. Notably, the enhanced precipitate density following LSP treatment amplifies these strengthening mechanisms by creating a higher density of these obstacles per unit volume, thereby producing a more pronounced hindrance to dislocation propagation throughout the material matrix.

3.5 Springback

Fig.13 shows the macroscopic profiles of creep-aged sheets with and without LSP treatment. Compared to the untreated sheet, the LSP-treated sheet exhibits reduced springback. Specifically, springback decreases from 4.5 mm (untreated) to 2.8 mm (LSP-treated), corresponding to a reduction in springback ratio from 25.0% to 15.6%, which exhibits a decrease of approximately 37.6%. These results demonstrate that LSP pre-treatment significantly mitigates springback in creep-aged components. This improvement is attributed to enhanced creep deformation during forming, homogenized precipitate distribution, and refined precipitates, which collectively increase the hardness and strength of the creep-aged alloy. The enhanced creep deformation is linked to the superposition of residual compressive stress induced by LSP and the compressive stress generated during bending at the concave surface of the sheet. LSP treatment imposes greater compressive stress on the concave surface compared to the untreated condition. Prior studies[3,25] have established that higher applied stress in Al-Li alloys leads to greater creep deformation. In this study, the increased compressive stress at the concave surface drives higher overall creep deformation. Unlike elastic deformation, creep deformation is irreversible and permanent. Consequently, the larger creep deformation in the LSP-treated sheet results in reduced springback after forming.

In summary, the springback suppression mechanism induced by LSP can be attributed to three synergistic effects. (1) Stress superposition-induced creep activation: the residual compressive stress field generated on the sheet surface

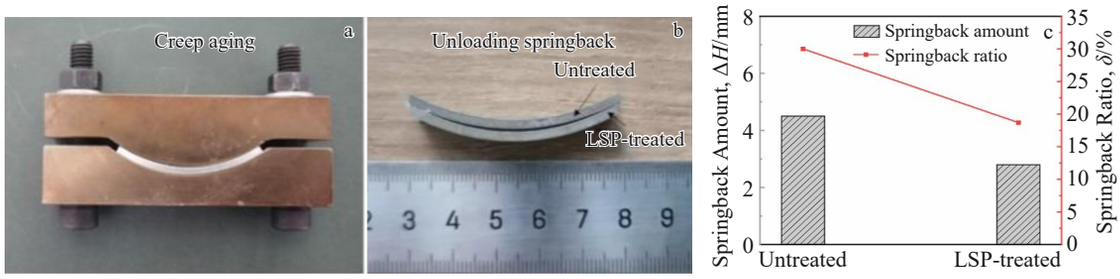

Fig.13 Creep aging device (a); untreated and LSP-treated specimens after unloading (b); comparison of springback amount and springback ratio between untreated and LSP-treated specimens (c)

through LSP interacts synergistically with the bending-induced compressive stress field. This combined stress state exceeds the critical threshold for dislocation glide, thereby producing plastic deformation and activating enhanced creep deformation that consumes elastic strain energy and reduces springback propensity. (2) Irreversible deformation dominance: LSP-induced dislocation substructures promote the conversion of reversible elastic strains into irreversible creep strains through thermally activated dislocation glide or climb mechanisms during creep aging. This energy dissipation pathway effectively reduces the elastic energy storage available for springback. (3) Precipitation strengthening effect: the aging process triggered by LSP facilitates the homogeneous nucleation of high-density fine nano-scale T1 precipitates within the alloy matrix. These coherent precipitates create strong pinning effects on dislocations, increasing the yield strength of material and consequently improving dimensional stability against springback.

4 Conclusions

1) The creep-aged 2195 aluminum-lithium alloy with LSP treatment exhibits a 22% increase in hardness compared to that without LSP treatment. This enhancement is attributed to grain refinement strengthening and precipitation strengthening induced by LSP.

2) Both LSP-treated and untreated creep-aged alloys display a gradient distribution of grain sizes from the surface to the intermediate layer. However, the LSP-treated alloy shows smaller grain sizes across all layers compared with untreated alloy. The largest difference in grain size occurs at the surface layer (49 μm), while the smallest difference is observed in the intermediate layer (4 μm). This confirms that LSP treatment effectively refines grain structure, contributing to grain refinement strengthening.

3) Nano-sized T1 (Al_2CuLi) precipitates are observed in both processing routes. However, LSP-treated alloy exhibits a higher density, finer distribution, and a 59.5% reduction in average precipitate size (from 126 nm to 51 nm). These refined precipitates enhance material strength and hardness through precipitation strengthening.

4) LSP treatment reduces the springback ratio of creep-aged sheets by 37.6% (from 25.0% to 15.6%). This reduction mainly stems from the synergistic effect of residual compressive stress (introduced by LSP) and bending-induced compressive stress at the concave surface. This combination promotes significant permanent creep deformation during aging, thereby minimizing elastic recovery. These findings provide a novel strategy for manufacturing high-strength and low-springback Al-Li alloy components in aerospace applications.

References

1 Liu Q, Chu S J, Zhang X *et al*. *Journal of Materials Science & Technology*[J], 2025, 209: 262
2 Zhang H K, Shang J H, Ma H C *et al*. *Applied Surface Science*[J], 2025, 698: 163067
3 Zhang L W, Li H, Bian T J *et al*. *Materials Science and Engineering A*[J], 2023, 865: 144615
4 Zhan L H, Lin J G, Dean T A *et al*. *International Journal of Machine Tools and Manufacture*[J], 2011, 51(1): 1
5 Zhang L W, Li H, Bian T J *et al*. *Chinese Journal of Aeronautics*[J], 2022, 35(10): 8
6 Yang Y L, Zhan L H, Ma Q Q *et al*. *Journal of Materials Processing Technology*[J], 2016, 229: 697
7 Xu G F, Liu M J, Liu S C *et al*. *Journal of Materials Research and Technology*[J], 2024, 30: 9037
8 Zhu H X, Ma P P, Liu C H *et al*. *Journal of Materials Research and Technology*[J], 2022, 20: 3471
9 Zuiko I, Kaibyshev R. *Journal of Alloys and Compounds*[J], 2024, 976: 173200
10 Wang C C, Quan L W, Su H H *et al*. *Materials Science and Engineering A*[J], 2025, 935: 148334
11 Li K Z, Wang Y Z, Su R M *et al*. *Journal of Alloys and Compounds*[J], 2025, 1022: 179970
12 Li Y, Shi Z S, Lin J G *et al*. *International Journal of Machine Tools and Manufacture*[J], 2018, 132: 113
13 Yang Y, Lian X L, Zhou K *et al*. *Journal of Alloys and Compounds*[J], 2019, 781: 330
14 Yang Y, Zhou K, Li G J. *Optics & Laser Technology*[J], 2019, 109: 1
15 Chen L, Li Y Z, Yu T Q *et al*. *Journal of Materials Processing Technology*[J], 2025, 335: 118667
16 Yilmaz A. *Science and Technology of Advanced Materials*[J], 2011, 12(6): 063001

17 Choi Y, Ha J, Lee M G *et al*. *Scripta Materialia*[J], 2021, 205: 114178
18 Wu C H, Li H, Bian T J *et al*. *Materials Today Communications*[J], 2023, 36: 106633
19 Xiao F, Wu M X, Wang Y X *et al*. *Transactions of Nonferrous Metals Society of China*[J], 2022, 32(4): 1061
20 Li G Q, Bai P C, Sun Y W *et al*. *Journal of Alloys and Compounds*[J], 2025, 1010: 177927
21 Ma P P, Liu C H, Chen Q Y *et al*. *Journal of Materials Science & Technology*[J], 2020, 46: 107
22 Wang Q W, Shao B, Qiu L P *et al*. *Materials Science and Engineering A*[J], 2025, 924: 147781
23 Zhang L, Liu C Y, Xie H Y. *Materials Characterization*[J], 2022, 194: 112472
24 Li C L, Mei Q S, Li J Y *et al*. *Scripta Materialia*[J], 2018, 153: 27
25 Zhang L W, Li H, Bian T J *et al*. *Chinese Journal of Aeronautics*[J], 2025, 38: 103165
26 Yang X X, Wang J S, Zhang M S *et al*. *Materials Today Communications*[J], 2021, 29: 102898
27 Ma P P, Zhan L H, Liu C H *et al*. *Materials Science and Engineering A*[J], 2021, 802: 140381
28 Li H, Zhan L H, Huang M H *et al*. *Journal of Alloys and Compounds*[J], 2021, 851: 156829
29 Song J D, Luo S H, Liang X Q *et al*. *International Journal of Fatigue*[J], 2022, 155: 106588
30 Jia M Y, Wang Y L, Yue J F *et al*. *Surfaces and Interfaces*[J], 2024, 44: 103757
31 Liu Z Y, Zha R W, Tan Z J *et al*. *Vacuum*[J], 2025, 232: 113848

激光冲击处理对2195铝锂合金蠕变时效行为及回弹的影响

张力文[1]，边天军[1]，龚小涛[1]，崔英帼[1]，宋继萍[2]
(1. 西安航空职业技术学院，陕西 西安 710089)
(2. 中国飞行试验研究院，陕西 西安 710089)

摘　要：采用硬度测试、微观组织表征和蠕变时效成形实验研究了激光冲击处理对2195铝锂合金蠕变时效行为的影响，并探讨了激光冲击处理对蠕变时效成形单曲率构件回弹的影响。结果表明，相比于未经激光冲击处理的蠕变时效合金，经激光冲击处理后的蠕变时效合金硬度值提升约22%，且晶粒尺寸从板材表层到中间层显著降低，其中表层晶粒尺寸在2种工艺处理后的差异最大（49 μm），中间层晶粒尺寸的差异最小（4 μm）；经激光冲击处理的蠕变时效合金内部的T1析出相分布更密集，数量更多，尺寸更细小。此外，经激光冲击处理的蠕变时效成形板材，与未经过处理的板材相比，其回弹率明显下降，降低幅度约37.6%。硬度提升归因于激光冲击带来的细晶强化和显著的析出强化，回弹率的降低是由于激光冲击处理后的板材凹面在弯曲过程中受到的压应力与激光冲击产生的残余压应力共同作用而产生了更大的蠕变变形。

关键词：激光冲击；蠕变时效；回弹；析出强化

作者简介：张力文，男，1989年生，博士，副教授，西安航空职业技术学院，陕西 西安 710089，电话：029-86855712，E-mail：npuzlw@mail.nwpu.edu.cn